OPTOELECTRONİCS AND ADVANCED MATERİALS – RAPİD COMMUNİCATİONS Vol. 2, No. 11, November 2008, p. 746 - 750

Structure and magnetic properties of electrodeposited ZnFeNi alloys

I. HAKKI KARAHAN[*], A. EKICIBIL[a]
Department of Physics, Faculty of Art and Science, Kilis 7 Aralık University, Kilis/Turkey
[a]*Department of Physics, Faculty of Art and Science, University of Cukuruva, Adana/Turkey*

Zn-Fe-Ni films were fabricated on aluminum substrate under potentiostatic deposition condition and their composition, magnetic property and structure were evaluated as a function of $FeSO_4$ concentration in electrolyte. The bath was consisted of 40 g/l $ZnCl_2$, 10 g/l $NiCl_2.6H_2O$, (5 to 30) g/l $FeSO_4.7H2O$, 25 g/l $C_6H_5Na_3O_7.2H_2O$, 16 g/l H_3BO_3, 25 g/l NH_4Cl, 1 g/l gelatine. Cyclic voltammetry of Zn-Fe-Ni alloy was performed in to study electroplating process of the films. The structural and morphological properties of the as-deposited films were studied using X-ray diffractometer and scanning electron microscope. The films form with a high zinc content and show hexagonal close packed (HCP) structure with a strong (101) orientation. Magnetic properties were measured using a vibrating sample magnetometer. It is found that the composition, structure and magnetic properties of the thin films exhibit strong dependence on the composition of the bath electrolyte.

(Received September 15, 2008; after revision October 5, 2008; accepted October 27, 2008)

Keywords: Electrodeposition, Magnetic properties, ZnFeNi alloy

1. Introduction

Electrodeposited Zn-Ni [1-18] and Zn-Fe [19-21] alloys have been widely studied. Electrodeposition technique provides an economic alternative for potential applications. Binary Zn-Fe alloy coatings are characterized by excellent corrosion resistance, good weldability, good formability and good paintability. They have numerous important industrial applications in the chemical and galvanic process in the industry for automobile and aerospace industries. In addition, Zn-Fe alloy coatings with high iron content can serve as an effective undercoat for paints [22–25]. Polarization phenomena during Zn-Ni-Fe alloy electrodeposition in acidic chloride bath were studied by Younan et. al. [26]. The phase system of the Zn-Fe-Ni alloys were studied and lebeled [27-28].

It was found that the Zn-Ni-Fe alloy deposition acts anomalously like Zn-Ni deposition mechanisms [26]. The electrodeposition of Zn with Fe-group metals is classified as anomalous, since Zn deposits preferentially in most plating conditions.

In view of magnetization behavior, Zn-Fe-Ni alloys are unique in that the inclusion of the diamagnetic zinc atom in the ferromagnetic Ni-Fe system is expected to increase the ferromagnetic character instead of reducing the magnetic moment [29]. In this paper, we focus on the dependence of the composition, structure and magnetic properties of the electrodeposited Zn–Fe–Ni thin films on bath composition, and investigate their structure-property relation.

2. Experimental

Four Zn–Fe-Ni alloys were obtained by electrodeposition from a citrate bath. The pH values of electrolytes were maintained at 4 ± 0.05. The voltages of electrodepositions were -2.5 V. The plating time was 10 min, after which the cathode was withdrawn, washed with distilled water and dried. All these electrolytes were prepared from Merck pro-analysis grade chemicals and double-distilled water (18 MΩ cm). The substrates were aluminum foils. Substrates were mechanically and chemically cleaned. Counter electrode was a Pt gauze electrode. The reference electrode used in all experiments was an Ag/AgCl electrode. All the potentials are referred against this electrode.

Electrodeposition was performed with an electrochemical analyzer/workstation (Model 1100, CH Instruments, USA) with a three-electrode configuration. The electrolyte pH was adjusted to 4 by adding NaOH. The electrodeposition process was conducted at 45 ^oC without stirring. A Rigaku difractometer was used to analyze the structure of alloys. The X-ray difractometer was operated at 30 kV and 30 mA with CuKα radiation. An atomic absorption spectrophotometer (AAS) Perkin-Elmer was used to determine the film composition, after dissolving the deposits in concentrated hydrochloric acid and diluting the solution with distilled water to 100 ml. The results obtained AAS were shown in Table 1.

Table 1.. Chemical composition of deposits.

Electrolyte (g/l)			% at Electrolyte			% at Film		
Zn	Fe	Ni	Zn	Fe	Ni	Zn	Fe	Ni
1,6	0.2	0.4	72.7	9.1	18.2	93	3	4
1,6	0.4	0.4	66.7	16.7	16.7	92	5	3
1,6	0.8	0.4	57.1	28.6	14.3	88	10	2
1,6	1.2	0.4	50	37.5	12.5	80	17	3

The error for the elemental compositions in Table 1 is ±0.1%. The morphology of the deposits was analyzed by scanning electron microscopy (SEM). Magnetic properties were measured using a vibrating sample magnetometer (VSM).

3. Results and discussion

Fig. 1 shows a typical Cyclic Voltammetry curve of the Zn-Fe-Ni alloy on the aluminum substrate. When the scan was performed from 0.8 V to -2.0 V, a reductive peak was observed at -1.2 V. When the potential was scanned in the reverse direction (from -2.0 V in a positive direction) two stripping peak was found at -0.2 and 0 V. The first peak corresponds to the prefential dissolution of zinc and the second peak to nickel-rich phase.

The effect of $FeSO_4$ concentration on the preferred orientation of Zn-Fe-Ni deposits is shown in fig. 2. Depending on the chemical compositions the phases of the electrodeposited Zn–Fe-Ni alloy are very complicated. The electrodeposited Zn–Fe-Ni alloys have metastable structures as electrodeposited Zn-Fe alloys and many phases coexist over a wide range of composition. These XRD patterns indicate that the films are of a hexagonal close packed (HCP) structure. Increasing Fe concentration changes the preferred orientation from a (100), (101) to (101) (100) double texture. At the $Zn_{92}Fe_5Ni_3$ and $Zn_{93}Fe_3Ni_4$ films, only (100) and (101) peaks is observed. As the iron content increases to 10 and 17 %, Zn (002) peak appears. At 39.80^0, a new peak appeared for the three films except $Zn_{93}Fe_3Ni_4$. This phase was not identified. The analysis shows the peak positions shifts with the iron content. The phenomenon could be attributed to the formation of ZnFeNi alloys and / or the effect of stress created during the deposition.

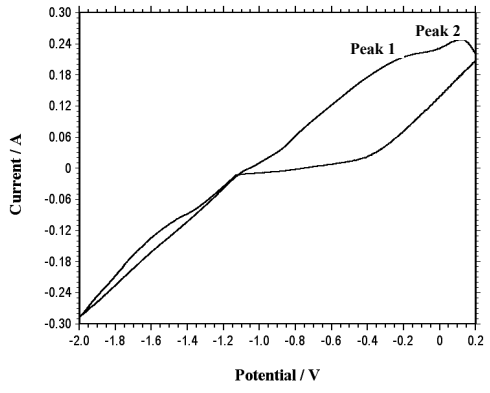

Fig. 1. Cyclic voltammetry of Aluminum substrate in presence of $ZnCl_2.5H_2O$ 40 g/l, $FeSO_4.6H_2O$ 10 g/l, $NiCl_2.5H_2O$ 10 g/l, $C_6H_5Na_3O_7{\cdot}2H_2O$ 25 g/l, H_3BO_3 16 g/l, NH_4Cl 25 g/l, Gelatine 1 g/l solution 45 °C. Scan rate:1 V/s.

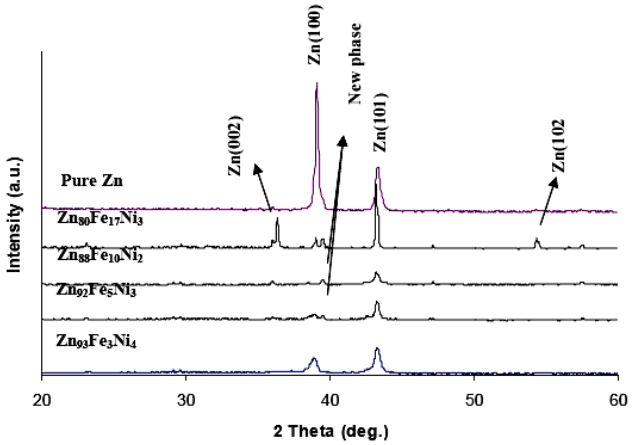

Fig. 2. XRD patterns of Zn-Fe-Ni deposits with various alloy content.

From the diffraction patterns ***a*** and ***c*** cell parameters of the hexagonal structure were found. (Fig. 3) The ***c*** parameter firstly decreased with the increase in the iron content; but a sudden change was observed when the iron percentage increased. On the other hand, the ***a*** parameter increased with the increase in iron content. However, for deposits with iron content greater than 10%, the lattice constant decreased at 0.26 nm.

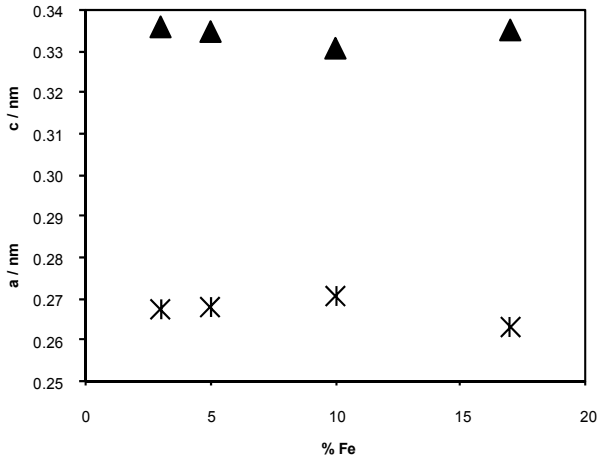

Fig. 3. Cell parameters for the ZnFeNi deposits with different iron percentages.

The grain size was analyzed by Scherrer's formula [30] (see Table 2).

The grain sizes were calculated for hcp (101) peaks. It firstly increased and then decreased with increasing iron content.

Table 2 shows that the magnetic content in the deposits increased in zinc matrix and increasing magnetic component increased the grain size of the alloys, except $Zn_{80}Fe_{17}Ni_3$ alloy. Addition of 7 at. % Fe leads to the diminishing of grain size of the zinc down to 20 from 24 nm.

Table 2. Parameters derived from the XRD patterns.

Sample	Peak type	Peak Position (^{o})	FWHM (^{o})	Grain size (nm)
$Zn_{80}Fe_{17}Ni_3$	Zn hcp (101)	43.252	0.440	20
$Zn_{88}Fe_{10}Ni_2$	Zn hcp (101)	43.253	0.358	24
$Zn_{92}Fe_5Ni_3$	Zn hcp (101)	43.209	0.385	22
$Zn_{93}Fe_3Ni_4$	Zn hcp (101)	43.297	0.420	21

Fig. 4 shows the dependence of the Fe concentration in the films on the Fe content in the bath electrolyte. Fe concentration increased with increasing bath Fe content. But zinc was deposited more preferentially. It is found that the amount of iron in deposit increases with the increase of Fe^{2+} concentration in the electrolyte but the compositions of alloys remain always lower than the composition reference line (CRL) defined as:

$$CRL = \frac{c(Fe^{2+})}{[c(Zn^{2+} + Fe^{2+} + Ni^{2+})]} \quad (2)$$

where $c(Fe^{2+})$, $c(Ni^{2+})$ and $c(Zn^{2+})$ are the concentrations of iron, nickel and zinc in electrolytes. It is showed from the figure that there is a slow increase in wt % Fe in deposit versus Fe concentration in the bath.

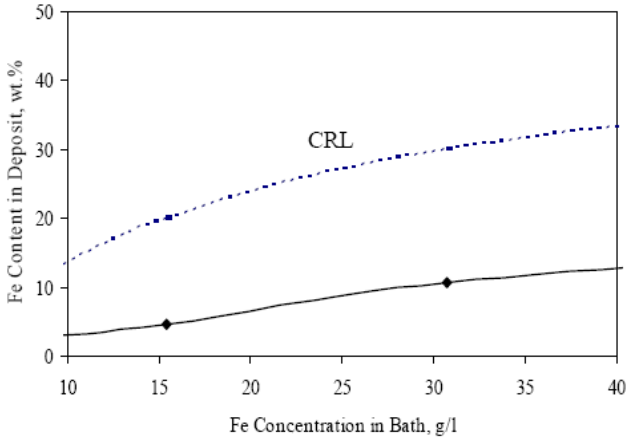

Fig. 4. Iron deposit content in thin films as a function of iron content at the electrolyte.

All the deposits obtained from the investigated solutions are well adherent to the steel substrate. The metallic luster and brightness of the deposit decreased with presence of iron. It is observed that the deposits are generally composed of fine grains. The surface morphology of the films was examined by SEM. Fig.5.a, b, and c. show SEM images for the as-deposited Zn-Fe-Ni alloys. The $Zn_{88}Fe_{10}Ni_2$ alloy (Fig. 5(b)) is very homogeneous and constructed of small particles showing no cracks as compared with the other films (Fig. 5(a) and (c)). The color of the films became dull with increasing the iron concentration of electrolyte.

The magnetic hysteresis loops of the electrodeposited ZnFeNi films was investigated at room temperature and the applied field is parallel to the film plane by VSM for four iron content of 10, 20, 30, 40 g/l, respectively. The compositional dependence of electrodeposited ZnFeNi alloy films on magnetization, at room temperature is shown in Fig. 6.

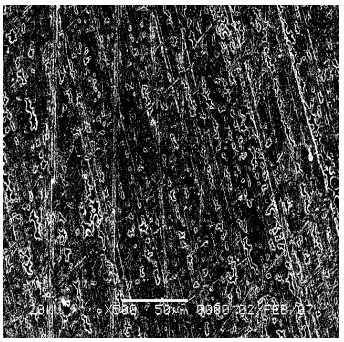

(a)

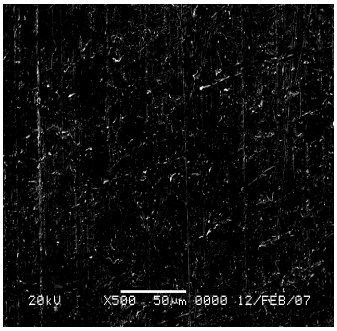

(b)

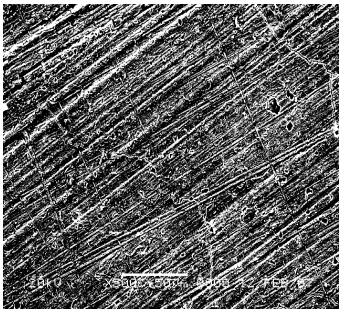

(c)

Fig. 5. (a) SEM image of $Zn_{93}Fe_3Ni_4$ alloy; (b) SEM image of $Zn_{88}Fe_{10}Ni_2$ alloy; (c) SEM image of $Zn_{80}Fe_{17}Ni_3$ alloy.

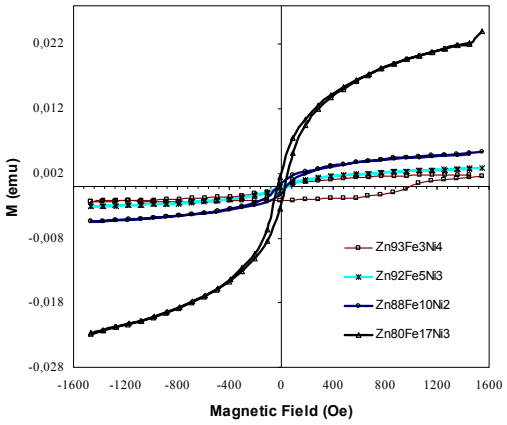

Fig. 6. Room temperature magnetization curves of ZnFeNi films.

For all sample values of H_c is much larger and values of saturation magnetization M_s are much smaller than those of the bulk materials, which may be due to the following factors: effect of the surface and interface may be first cause. The grain size of the samples much smaller than that of bulk materials, which induces an increase in the number of grain boundaries and then they act as pinning sites for domain walls [31]. And the defects in the film microstructure can effect H_c and the saturation magnetization M_s obviously [32, 33]. The second cause, the cation distribution in ZnFeNi thin films is different from that in bulk. For the films, the change of the H_c is not consistent with that of the bulk materials. As can be seen that high saturation magnetization M_s for the $Zn_{80}Fe_{17}Ni_3$ film, about 226 emu/g, was obtained, which was 4 to 10 times larger than that of other Zn-Fe–Ni alloys. In contrast, M_s for $ZnFe_2O_4$ film about 65 emu/g at low temperatures, (10 K) [34]. Magnetization under applied field increased with the magnetic component. The magnetic moments of the films are very low. Clearly, the films are ferromagnetic. The reason is that the coercivity and the roughness are strongly positively correlated. The changes in coercivity arise from the physical pinning of magnetic domains walls likely due to grain boundaries [35, 36].

4. Conclusions

We have fabricated the Zn-Fe-Ni films on the aluminum substrate by potentiostatic electrodeposition technique. The iron concentration of the thin films is a strong function the iron content of the bath electrolyte. The XRD analysis shows that the grain size reduces with decreasing Fe content at the deposits except for the $Zn_{80}Fe_{17}Ni_3$ film, explaining the decrease in the coercivity. The structure and magnetic property of Zn-Fe-Ni films could be tuned by adjusting the electrodeposition composition. The change of the H_c is not consistent with that of the bulk materials.

References

[1] A. Knodles, Ch. J. Raub, E. Raub, Metalloberflache, **39**(l), 21 (1985).
[2] G. N. K. Ramesh Babu, G. Devaraj, J. Ayyappa Raju, R. Subramanian, Metal Finish. **85**(2), 49 (1987).
[3] L. Felloni, R. Frateri, E. Quadrini, G. Rover, Journal of Applied Electrochemistrv. **17**(3), 574 (1987).
[4] D.E. Hal, Plating. 70(11), 59 (1983).
[5] M. F.Mathias, T. W. Chapman, Journal of the Electrochemical Society. **134**(6), 1408 (1987).
[6] I. Nonov, I. Gadehov, K. Pangarov, Galvanotechnik. **75**(9), 1107 (1984).
[7] R. G. Baker, C. A. Holden, Plating Surface Finish, **72**(3), 54 (1985).
[8] G. N. K. Ramesh Bapu, G. Devaraj, J. Ayyappa Raju, R. Subramaninan, Symposium on Industrial Metallic Finishes Abstracts, Karaikudi India, 32 (1985).
[9] A. Shibuya, T. Kurimoto, Y. Hoboh, N. Usuki, Transactions of the Iron and Steel Institute of Japan, **23**(11), 923 (1983).
[10] D. W. Sitari, M. Sagiyama, T. Hara, Transactions of the Iron and Steel Institute of Japan. **23**(11), 959 (1983).
[11] M. E. Soares, C. A. C. Souza, S. E. Kuri, Surface and Coatings Technology. **201**(6), 2953 (2006).
[12] M. E. Soares, C. A. C. Souza, S. E. Kuri, Materials Science and Engineering: A. **402**(1-2), 16 (2005).
[13] J. B. Bajat, V. B. Mišković-Stanković, Progress in Organic Coatings. **49**(3), 183 (2004).
[14] J. B. Bajat, Z. Kačarević-Popović, V. B. Mišković-Stanković, M. D. Maksimović, Progress in Organic Coatings. **39**(2-4), 127 (2000).
[15] G. Reumont, P. Perrot, J. Foct, J. Mater. Sci., **33**, 4759 (1998).
[16] S. O. Pagotto Jr., C. M. A. Freire, M. Ballester, Surface&Coating Tech. **122**, 10 (1999).
[17] H. Y. Lee, S. G. Kim, Surface&Coating Tech. **135**, 69 (2000).
[18] M. Gavrila, J. P. Millet, H. Mazille, D. Marchandise, J. M.Cuntz, Surface&Coating Tech. **123**, 164 (2000).
[19] İ. H. Karahan, J. Mater. Sci., **42**(24), 10160 (2007).
[20] Z. N. Yang, Z. Zhang, J. Q. Zhang, Surface &Coating Tech., **200**, 4810 (2006).
[21] C. J. Lan, W. Y. Liu, S. T. Ke, T. S. Chin, Surface & Coating Tech. **201**, 3103 (2006).
[22] D. Crotty, R. Grıffin, Plating & Surface Finishing, **83**(6), 23 (1996).
[23] H. Park, J. A. Szpunar, Corrosion Science **40**(4), 525 (1998).
[24] M. P. Gıgandet, J. Tachez, Surface Coating Technology, **89,** 285 (1997).
[25] Y. Lıao, , D. R. Gabe, C. D. Wılcox, Plating & Surface Finishing, **85**, 62 (1998).
[26] M. M. Younan, O. A. Fadali, I. H. M. Aly, T. Oki, Mater. trans. – JIM, **37**(12), 1763 (1996).
[27] V. Raghavan, J. Phase Equilib. **24**(6), 558 (2003).
[28] F. Peng, F. Yin, X. Su, L. Zhi, M. Zhao, J. Alloys Compd., **402**, 124 (2005).
[29] M. V. Ananth, N. V. Parthasaradthy, Int. J. Hydrogen

Energy, **22**(8), 747 (1997).
[30] B. D. Cullity, S. R. Stock, Elements of X-ray Diffraction, 3 rd ed., Prentice Hall, New Jersey, 170 (2001).
[31] J. M. D. Joey, Phys. Rev. Lett., **27**, 1140 (1971).
[32] J. P. Chen, C. M. Sorensen, K. J. Klabunde, Phs. Rev. B., **54**, 9288 (1996).
[33] M. Pal, P. Brahma, D. Chakravorty, J. Magn. Mater., **164**, 256 (1996).
[34] Changwa Yao, Qiaoshi Zeng, G. F. Goya, J. Phys. Chem. C, **111** (33), 12274 -12278, 2007.
[35] M. Taheri, E. E. Carpenter, V. Cestone, J. Appl. Phys., **91**, 7595 (2002).
[36] F. Zhang, Y. Kitamoto, M. Abe, J. Appl. Phys., **87**, 6881 (2000).

*Corresponding author: ikarahan@gantep.edu.tr